

# Army Research Laboratory

Aberdeen Proving Ground, MD 21005-5066

---

---

ARL-TR-2444

April 2001

---

---

## On the Flame Structure of RDX

Barrie E. Homan, Martin S. Miller, and John A. Vanderhoff  
Weapons and Materials Research Directorate, ARL

---

## Abstract

---

In an attempt to refine the database for the evaluation of detailed-chemistry combustion models, absorption spectroscopy has been applied to low pressure, self-deflagrating RDX flames. Semi-empirically determined production rates of reactants from the solid propellant surface, together with a detailed gas-phase elementary reaction set, were used to develop a model that minimizes the effect of uncertainties in the description of solid phase processes. The spatial profiles of two low concentration, highly reactive, short-lived diatomic species, CN and NH, were obtained at pressures varying from 1 to 2 atm in air. Two major species, NO and OH, were also profiled using this technique. The CN and NH profiles agree well with previous measurements and the current model. NO and OH profiles are also in good agreement with the models. During the course of these spectroscopic measurements, burning rates for RDX over a pressure range of 1–2 atm have also been determined. These values range from 0.23 mm/s at atmospheric pressure to 0.50 mm/s for 2 atm and are noticeably lower than some of the other published measurements. Calculations stemming from the proposed model predict a burning rate of 0.29 mm/s and 0.54 mm/s for the same pressure levels.

## Acknowledgments

We thank Dr. Anthony Kotlar for developing the least squares fitting programs and the necessary molecular database files for OH, NO, CN, and NH.

INTENTIONALLY LEFT BLANK.

# Table of Contents

	<u>Page</u>
<b>Acknowledgments</b> .....	iii
<b>List of Figures</b> .....	vii
<b>List of Tables</b> .....	ix
<b>1. Introduction</b> .....	1
<b>2. Experiment</b> .....	2
<b>3. Data Analysis</b> .....	8
<b>4. Model</b> .....	10
<b>5. Results</b> .....	16
5.1 Absorption.....	16
5.2 Video Records.....	24
5.3 Burning Rate .....	25
<b>6. Discussion</b> .....	27
<b>7. Conclusions</b> .....	30
<b>8. References</b> .....	33
<b>Distribution List</b> .....	37
<b>Report Documentation Page</b> .....	41

INTENTIONALLY LEFT BLANK.

## List of Figures

<u>Figure</u>		<u>Page</u>
1.	Experimental Setup .....	3
2.	Triple-Pass Beam Path.....	5
3.	0.794-mm Diameter, 1-atm Air Self-Deflagrating RDX .....	8
4.	Pyrolysis Law.....	11
5.	Specific Heat of RDX.....	13
6.	RDX Species Model Profiles .....	15
7.	OH Concentration Profile at 1 atm.....	17
8.	OH Concentration Profile at 2 atm.....	18
9.	1-atm Temperature Profile for RDX .....	18
10.	2-atm Temperature Profile Obtained From OH Spectra .....	19
11.	CN Spectrum for 1 atm, 0.7 mm From Sample Surface.....	19
12.	CN Concentration Profile at 1 atm.....	21
13.	NH Profiles in 1-atm Air.....	22
14.	High Resolution Profiles of CN and NH at 1 atm.....	23
15.	High Resolution NO Species Profiles.....	24
16.	Temperature Profile From NO Spectra at 1 atm.....	25
17.	Burn Rate of RDX as a Function of Pressure .....	26

INTENTIONALLY LEFT BLANK.

## List of Tables

<u>Table</u>		<u>Page</u>
1.	Semi-Empirical Model Parameters .....	14
2.	Comparison of CN and NH Concentrations Obtained in the Self-Sustained Combustion of RDX.....	22
3.	Video Measurements for RDX Burning in Air .....	25
4.	Comparison of NO Concentrations at 1-atm Air .....	29

INTENTIONALLY LEFT BLANK.

# 1. Introduction

Over the last several years, propellant combustion models, including detailed gas-phase chemistry, have been developed for cyclotrimethylene trinitramine (RDX) and cyclotetramethylene tertranitramine (HMX) propellants [1-7]. These models attempt to describe the generation of gas phase reactants as a combination of evaporation from the surface and subsurface molecular decomposition [2, 4, 8, 9]. While the usual combustion diagnostic data, such as temperature and species concentration profiles, are predicted by these calculations, the more important parameter they strive to predict is the rate of burning as a function of pressure. Burning rate measurements for RDX exist in the literature, and current models show that excellent agreement can be achieved. Unfortunately, some of the necessary physical and chemical parameters and mechanisms used to describe the solid gas-phase transition are not known with a high degree of certainty. Hence, "excellent" agreement should be viewed with this in mind. A new semi-empirical model that minimizes the need for a detailed description of the condensed phase processes has been developed; it will focus on the chemistry of the gas phase.

In addition to burning rate measurements for RDX, there is also an accumulation of other quantitative combustion diagnostic measurements. Thermocouple [7, 9], mass spectrometric [10, 11], and optical measurements [12-16] constitute the majority of measurements which produce temperature and concentration profiles for RDX combustion. Over the last eight years, the U.S. Army Research Laboratory (ARL) has been using absorption spectroscopy in an effort to expand and refine the combustion diagnostic database for propellants and propellant ingredients. In some early studies [17, 18], concentrations of CN, NH, and OH species were determined from absorption spectra taken during the self-sustained combustion of the solid propellants M-30 and HMX1.\* The measurements were reported with the caveat that these concentrations should not be considered maximum values due to uncertainties in path length. Previous experiments [12, 13], as well as modeling results [1, 2, 9] for RDX, have indicated that the spatial extent of CN, NH, and NO is within approximately 1 mm from the surface of the

---

\*Composition of HMX1 is 73% HMX, 17% Trimethylolethanetrinitrate, and 10% polyester binder.

propellant at atmospheric pressure and decreases with increasing pressure. Therefore, measurements of CN, NH, and NO require a high degree of spatial resolution for the detection system. In addition, the combustion process must exhibit a high degree of one-dimensionality if species profiles are to be measured with a line-of-sight technique. Spatial coincidence of the thin combustion region containing these short-lived species and the probing beam is critical, as any misalignment can reduce the apparent measured concentration. OH does not suffer from these limitations as the concentration slowly varies in the secondary flame region.

In these early studies, the propellant was ignited by a hot wire placed at the center of the sample. Thus, burning propagates from the sample center. A shroud gas flowing around the propellant to eliminate side burning and to keep the absorption path length free of contaminants also provided an unwanted edge cooling effect. A visual examination of some propellant samples that self-extinguished when burning near the low pressure deflagration limit revealed that the burning surface was not flat, but rather concave. This surface feature was not detectable with the video camera arrangement employed for those experiments. The resultant nonplanar burning was thought to be the major factor resulting in low measured concentrations. For these reasons, subsequent experiments focused on propellants with large dark-zone regions [19–21], where the spatial resolution requirements are much less.

Recently, attention has again been turned to obtaining CN, NH, NO, and OH concentration measurements. The RDX monopropellant was chosen for the study because of recent community interest in modeling this system. An additional factor considered was that this monopropellant forms a liquid layer during combustion, and this phase would give a more planar burning surface. In this report, concentration profiles and burning rate measurements, together with new model predictions, are compared to results obtained from the literature.

## 2. Experiment

The optical absorption experiment previously described [17–21] has been modified and improved significantly. The new experiment setup is shown in Figure 1. Originally, a hot wire

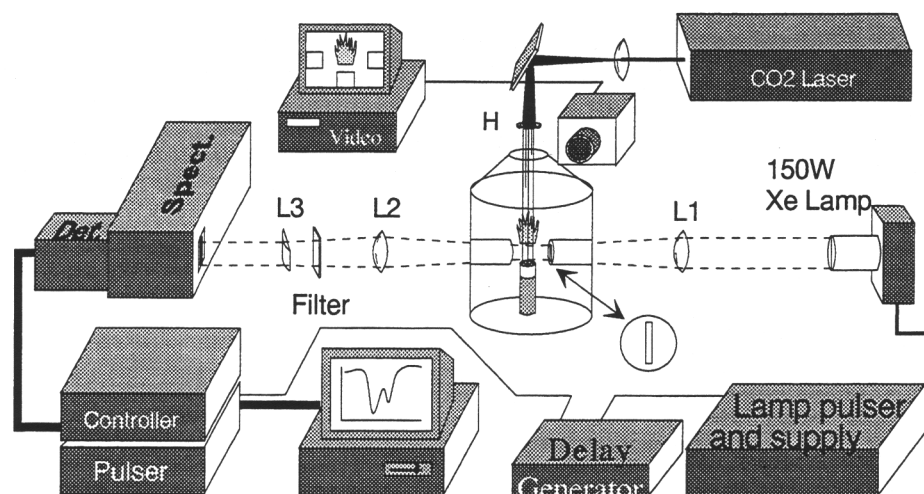


**Figure 1. Experimental Setup.**

was used to ignite the propellant samples [17–19], but was later replaced by a Synrad Model D48-2 25 Watt CO<sub>2</sub> laser ignition source [20, 21]. The beam from this CO<sub>2</sub> laser was directed from the laser to the top center of the propellant sample via a ZnSe window located at the top of the previously described combustion vessel [18]. The total path of the CO<sub>2</sub> laser beam was about 70 cm, and it impacted about a 0.2-cm diameter area on the top center of the propellant sample. In an attempt to produce uniform ignition over the entire sample-end surface, a more powerful Synrad Model 57-1 100 Watt CO<sub>2</sub> laser was substituted. The ignition beam path length was originally extended to about 600 cm with three high-power Cu bending mirrors to take advantage of the uniform far-field beam profile. Because the loss from the mirrors was over 50%, the path length was shortened to the present length of 100 cm, and the number of mirrors was reduced to one. To compensate for the nonuniform beam profile, a ZnSe multifaceted optic (H) was included in the beam path to produce sixteen focused ignition points evenly distributed over about 75% of the propellant sample surface.

Two different absorption spectroscopy configurations were used in this experiment. In the “snapshot” configuration, separate spectra corresponding to the distance into the combustion region were collected simultaneously within a 1-ms exposure [22]. Increasing the absorption probe light intensity, accomplished by pulsing the lamp and reducing the gain settings on the detector, was done to minimize the emission signal collected. In this mode, source light

intensities were increased about two orders of magnitude by applying a 75-V pulse to the simmering arc lamp, which provided the greatest benefit at shorter wavelengths. Increased emission light gathering, inherent in the snapshot experimental setup, was further addressed by introducing a shutter into the optical path prior to the combustion chamber. Emission spectra obtained with the shutter in the closed position are then used to correct the absorption spectra. The path length in the vessel, located outside the combustion region, was reduced by arms that extend into the vessel. These arms are adjusted to be slightly larger than the RDX sample diameter, and they trim the absorption light to a vertical sheet. Quartz windows glued to the ends of these arms seal the vessel while allowing transmission of UV-visible light. Another modification, shown in Figure 2, involved mounting these windows at a slight angle to the beam and mirroring a portion to produce multiple passes through the sample area within the pressure vessel. Vacuum deposition of Al on partially masked quartz substrates allowed for the triple pass arrangement and increased the absorption path length by about a factor of three. Initially, the mirrored side of the quartz windows faced inside to minimize interface losses. Unfortunately, these delicate surfaces were degraded by the combustion process and required replacement every two or three runs. In the present configuration, the windows have been flipped so that the mirrored surface is protected by the quartz substrate, thus eliminating the need for frequent replacement. Upon exiting the chamber, the light is imaged onto the spectrometer entrance slit with spherical lens L2 (Figure 1). The addition of a cylindrical lens L3 further focussed the light into a line coincident with the spectrometer slit. An appropriate bandpass filter is also included in the light path to provide more stray light rejection.

Because of the large temperature gradient near the propellant surface, beam steering is a concern for optical diagnostic techniques in combustion processes [23]. This effect may cause the beam to sample different regions in the flame as well as steer the output off of or onto different regions of the detector collection area. A fiber optic ribbon cable was included in the collection optics for one experiment to provide a way to isolate the cross talk of adjacent detector regions. The custom-made fiber consisted of 20 fibers with 200- $\mu\text{m}$  cores, 280- $\mu\text{m}$  center to center. One end of the fiber was placed within  $\approx 1.5$  cm from the center of the propellant sample, thereby significantly reducing the effective lever arm of the collection optics.

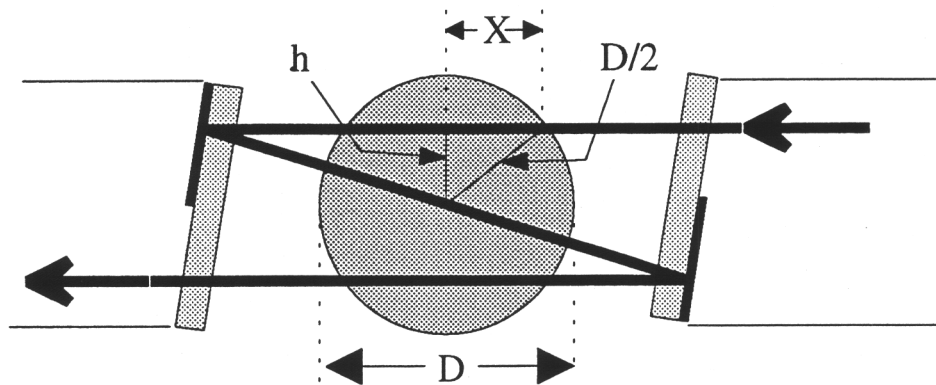


**Figure 2. Triple-Pass Beam Path.**

CN, NH, and NO exist within a region of approximately 1 mm from the surface of the propellant. To improve on the measurement of these species, the spatial resolution of the absorption measurement system was increased to  $\sim 100 \mu\text{m}$  by replacing the snapshot configuration with a more conventional high-resolution, single-beam experimental setup. As the spectra must be acquired sequentially, the rate of data frame collection becomes increasingly important. Pulsing the light source reduces the spectrum collection rate due to the finite charging time for the pulse capacitor. Therefore, the lamp was operated in a nonpulsed mode. For CN and NH, an appropriately modified version of the previously mentioned triple-pass experimental setup was used. This arrangement replaces the chamber and its mounted flat mirrors with concave mirrors to provide a higher throughput and improved spatial resolution. However, the use of concave mirrors precluded measurements made at other-than-atmospheric pressures. Because a triple-pass measurement of the NO (0,0) band would result in saturated absorption signal levels, a single pass setup was substituted for the measurement of this species.

The spectrometer is an Acton Research Co. SpectraPro 275 imaging spectrometer with a focal length of 0.275 m and entrance slits varying between 50 and  $100 \mu\text{m}$ . A 1200 groove/mm grating is used to wavelength disperse the light onto a Princeton Instruments Model 576T thermo-electrically cooled intensified charge coupled device (ICCD) array detector. The detector is externally gated and is sensitive only when a pulse is applied to the intensifier. This feature allows for short exposures of the detector to be controlled by a pulser and timed to

overlap the 1-ms light pulse of the xenon arc lamp. This detector is a two-dimensional (2-D) array with  $578 \times 385$  pixels oriented such that the 578 pixels are along the horizontal (wavelength) axis. The snapshot experiments have the 385 pixels in the spatial direction divided into regions either 16 or 32 pixels wide, giving 24 or 12 spectra, respectively. Thus, the distance covered and the spatial resolution depends on the number of vertical pixels summed and the magnification of the optics to the detector. This magnification is controlled by the distance between lens L2 and the sample. In this case, the range covered is 0.25 cm, and the spatial resolution is 0.021 cm. The spatial resolution is checked by moving a razor blade through the vertical absorption light sheet at the position that the sample would occupy and recording the micrometer drive settings at the point where the count rate drops to one half for each of the strips. Care was taken to ensure that cross talk between adjacent strips was minimal. Multiple, spatially distinct absorption spectra are recorded for each pulse of the absorption lamp. In reality, the initial position of the RDX sample is adjusted to block one or more of the strips during the first lamp pulse. This configuration assists in locating the propellant surface. In the case of the single probe beam absorption measurements, the detector had all of the vertical pixels summed into one super pixel. The same spatial resolution measurement apparatus is used here, except the profile of the single beam is obtained. A Gaussian function was fitted to the derivative of this profile to yield full-width-half-max (FWHM) values of 0.006–0.009 cm.

The 0.8-cm diameter RDX sample could not be made to reliably burn in a 1-atm nitrogen environment. Ulas et al. [16] also reported this behavior for their 0.64-cm diameter RDX samples; the lowest reported nitrogen pressure for which RDX combustion data was taken was 1.7 atm. The 1-atm measurements reported here were performed in air to overcome this limitation and to take advantage of the larger reaction zone. Present measurements (discussed in the results section) indicate that RDX has a burning rate of 0.023 cm/s in 1-atm air. The time required to obtain the spatially resolved absorption spectra is the duration of one pulse, or 1 ms. During this time period, the propellant would move less than 1  $\mu\text{m}$ . However, if more than one pulse is to be used for data, then movement of the propellant surface should be taken into account. A full data collection cycle consists of exposure, plus the time required to read the detector. For the 12-strip configuration, this time is  $\sim 150$  ms. Furthermore, if an emission

spectrum is required for each absorption spectrum, the cycle time is doubled, effectively limiting the pulse rate of the arc lamp to 3 pulses/s. In this situation, the propellant surface moves about 80  $\mu\text{m}$  between pulses. In high-resolution mode, the collection cycle is reduced to  $\sim 130$  ms total, with the sample surface regressing approximately 30  $\mu\text{m}$  between spectra.

Emission lines from Mercury and Neon pen lamps were used to calibrate the wavelength scales and determine the spectral resolution for the system. Measured spectral resolutions are determined for each experimental configuration. As an example, one configuration using a 100- $\mu$  spectrometer entrance slit had a measured spectral resolution (FWHM) of 0.35 nm. These values, incorporated in a Lorentzian lineshape, were input parameters for least-squares fitting the absorption spectra.

For these studies, cylindrical samples of RDX were prepared by pressing recrystallized RDX powder to about 540 MPa, or 96.9% of theoretical maximum density (TMD) into a cylindrical die of 0.794-cm diameter. A drop of methanol in the powder mixture allowed intact extraction of the pressed RDX pellets. A diamond saw cut these pressed RDX samples to the final thickness, typically 0.2 cm. These pellets were then put in a vacuum desiccator for 12 or more hours. In the past studies [17–21], an adjustable flowing nitrogen purge gas maintained constant pressure and provided a shroud gas flow around the burning propellant sample. To approximate a constant pressure, the propellants were either burned in open air or in a combustion vessel connected to a gas cylinder of sufficiently large volume (44 liter). Since there is no gas flow, a coating must be applied to the sides of the RDX samples to inhibit edge burning. A clear fingernail polish (Wet 'n' Wild) was used. As seen in Figure 3, this technique produced a flat burning surface with a rounding of the edges.

Video recordings were made for each experimental run. A Cohu Model 8210 color video camera operating in standard VHS or SVHS modes, connected to a Panasonic Model AG-1830 video cassette recorder and a Sony Model PVM-1341 color monitor, provided visual and tape recordings of each experiment. A Nikon 105-mm microlens coupled to the camera magnified the burning RDX samples to about 15X. A representative video frame of RDX combusting in

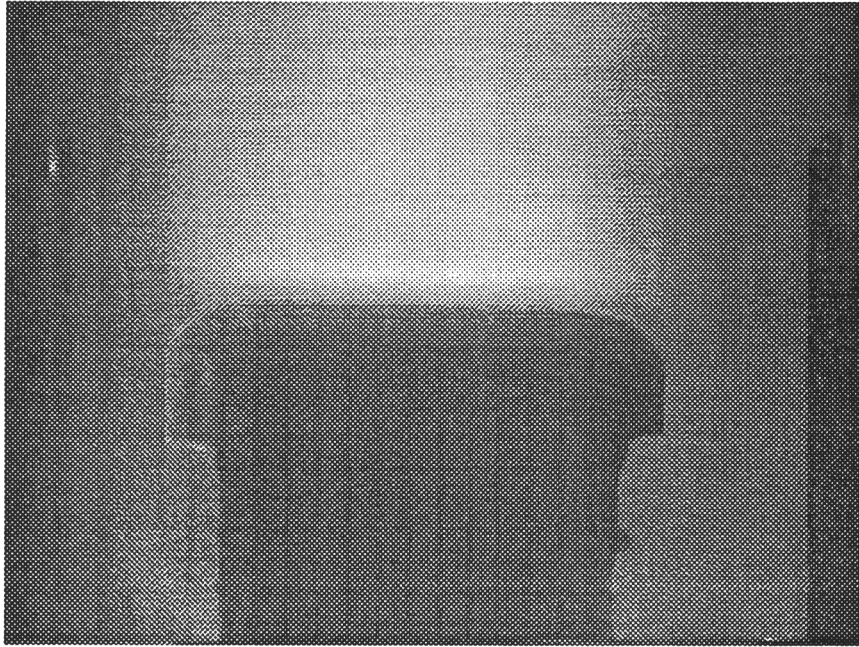


**Figure 3. 0.794-mm Diameter, 1-atm Air Self-Deflagrating RDX.**

1-atm air is shown in Figure 3. With the exception of the edges, this burn is flat to within 0.01 cm. Final concentration values are reported after a path length correction that compensates for edge and other nonplanar geometry. These adjustments can be as high as 50% due to the triple-pass experimental arrangement. Flame structure information can also be obtained from Figure 3. This picture shows a nonluminous zone of about 0.03 cm, starting at the propellant surface. The region at the base of the final flame zone is purple in color and is believed to be from a CN (0,0) emission band near 388 nm. In addition to flame structure and other 2-D information, the burning rate as a function of pressure is also obtained from these video recordings.

### **3. Data Analysis**

The governing equations for absorption have been described previously [17] and are briefly described here. Assuming a Boltzmann distribution of states and the differential absorption law,

$I(\nu)$ , the transmitted intensity of light at frequency  $\nu$  is attenuated along a path of length  $L$ , according to

$$I(\nu) = I_0 B(\nu) \exp[-k_\nu L], \quad (1)$$

where  $I_0$  is the initial intensity,  $k_\nu$  is the absorption coefficient of the molecule of interest, and  $B(\nu)$  is a baseline correction factor for any broadband attenuation along the path length. For the present conditions where the light source and the spectrometer bandwidths are much larger than the width of the absorption line, an instrument function,  $S(\nu, \nu_0)$ , centered at  $\nu_0$ , is introduced to give

$$I_t = \int S(\nu, \nu_0) I(\nu) d\nu, \quad (2)$$

where  $I_t$  is the integrated light transmitted. The instrument function for the detection system is obtained from low-pressure lamps described in the experimental section, and the molecular transition lineshape is approximated by a delta function. Molecular parameter and transition information have been tabulated previously [18] with appropriate references. The calculation of fractional absorption for CN in this reference considered only the (0,0) and (1,1) vibrational transitions occurring in the  $B^2\Sigma - X^2\Sigma$  electronic system. In the present calculations, the (2,2), (3,3), and (4,4) transitions are also included. Franck-Condon factors for these transitions are taken from Suchard [25], where  $q_{22} = 0.64884$ ,  $q_{33} = 0.57392$ , and  $q_{44} = 0.52453$ . Effects of the perturbation for the (4,4) transition of CN are not considered. Using initial guesses for temperature and molecular concentration for a given species of interest,  $I_t$  can be calculated from equation 2. These calculations are adjusted and compared with the experimental measurements of the transmitted light in a nonlinear, multivariate, least-squares fitting program in which the concentration, temperature, wavelength calibration, and baseline parameters are allowed to vary.

Soon after propellant ignition, the flame begins to migrate down the sides of the sample (Figure 3), despite the application of a nail polish (cellulose acetate) inhibitor. The narrow profile of the intermediate species near the dark zone closely follows the surface contour. As shown in

equation 1, the product of the absorption coefficient,  $k_v$  (proportional to concentration), and the path length  $L$ , is constant for a given transmission. The rounding of the edges in an otherwise flat combustion region results in a reduced effective path length available for a line-of-sight technique. To correct this, the mole fraction obtained by the fit, which is linearly dependant on the path length, was increased by the ratio of uncorrected to corrected path lengths. The corrected path length in the dark zone combustion region was determined by measuring the flat portion of the violet emission from CN. Assuming that this emission delineates the horizontal extent of the combustion zone for other species in this region, the effective path lengths for NO and NH were also taken to be the same as that of CN. For the triple-pass experiment, the correction can be as high as 50%. Because the concentration of OH peaks much further into the final flame zone, the path length was taken as the width of the propellant sample.

## 4. Model

We have developed a new burning-rate model [26], which may be particularly suited to testing the gas-phase reaction mechanism by comparing experimental and theoretical species profiles. This model treats the gas phase at the level of complex elementary-reaction networks. In the condensed phase, the linear surface regression rate ( $r$ ) is assumed to be related to the surface temperature ( $T_s$ ) by the following semi-empirical relationship:

$$r = A_s e^{-\frac{E_s}{RT_s}} \quad (3)$$

This expression, known in the propellant-combustion literature as the pyrolysis law, can be derived for surface regression due to condensed-phase reactions in certain limiting cases [7, 27]. Zenin [28] has shown that this relation gives a good account of his data for double-base propellants, for which the regression mechanism is probably reactive. A linearized least-squares fit of this relationship to the data of Zenin [7] for RDX is shown in Figure 4; the good fit illustrates that it also works well when the regression mechanism is evaporative. We assume in

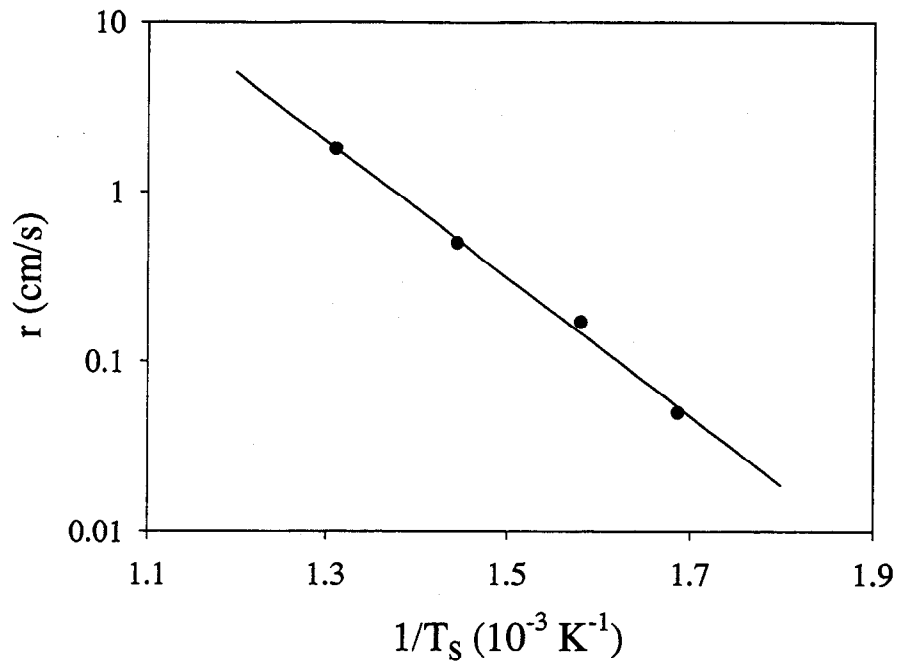


**Figure 4. Pyrolysis Law.**

this model that there are no reactions occurring in the bulk liquid, even though both exothermic and endothermic surface gasification mechanisms are permitted. These two mechanisms distinguish themselves in the enthalpy of the products relative to the starting material.

The pyrolysis law specifies the rate at which reactants for the gas phase are formed. The identity and mole fractions of these reactants, as created at the surface, must also be known. Liao and Yang [2] and Liao [9] modeled two condensed-phase reactions by which RDX may decompose, but their calculations showed that little decomposition of RDX actually occurred there. Therefore, we assumed that the gas-phase reactant leaving the surface was all vapor-phase RDX.

The boundary conditions on the chemical species mass fractions ( $Y$ ) at the liquid/gas interface are as follows:

$$\dot{m}Y_i^{-0} = \dot{m}Y_i^{+0} + \rho_g Y_i^{+0} V_i^{+0}, \quad (4)$$

where  $i$  is the index denoting the  $i$ th chemical species,  $\pm 0$  denotes the condensed (-) and gas (+) phase boundary conditions,  $V_i$  is the diffusion velocity,  $\rho_g$  is the gas phase mass density, and  $\dot{m}$  denotes the mass flux related to the linear burning rate and surface density by

$$\dot{m} = \rho_s r. \quad (5)$$

Molecular diffusion in the condensed phase is neglected. In terms of this notation, our previous assumption that the “product” of pure, liquid-phase RDX “decomposition” is vapor-phase RDX is expressed as

$$Y_{\text{RDX}}^{-0} = 1. \quad (6)$$

Assuming no condensed-phase molecular diffusion, the boundary condition on energy flux at this interface is

$$\lambda_c \left( \frac{dT}{dx} \right)^{-0} - \sum_i \dot{m} Y_i^{-0} h_i^{-0} = \lambda_g \left( \frac{dT}{dx} \right)^{+0} - \sum_i \dot{m} Y_i^{+0} h_i^{+0} - \sum_i \rho_g Y_i^{+0} V_i^{+0} h_i^{+0}. \quad (7)$$

The thermal conductivity in the condensed and gas phases at the surface is represented by  $\lambda_c$  and  $\lambda_g$ , and  $h_i$  is the specific enthalpy of the  $i$ th species. By further assuming there are no bulk liquid reactions, the species boundary conditions can be combined with the energy conservation equation in the condensed phase. By integrating over the interval  $(-\infty, -0)$ , the energy boundary condition at the interface between the gas and condensed phases becomes

$$\lambda_g \left( \frac{dT}{dx} \right)^{+0} = \dot{m} \sum_i (Y_i^{-0} h_i^{+0} - Y_i^{-\infty} h_i^{-\infty}). \quad (8)$$

This form of the boundary condition is very useful because the thermophysical properties of the condensed phase at any temperature other than the initial temperature need not be known, at

least for purposes of finding the burning-rate eigenvalue. Of course, if the temperature profile in the condensed phase is desired, these properties at all temperatures between  $T_0$  and the surface temperature  $T_s$  must be known.

The enthalpy of the condensed phase at the initial temperature was determined as follows. The specific heat of solid RDX was obtained by a least-squares fit of a linear temperature function to the data of Shoemaker et al. [29] and Miller [30]. The fit is shown in Figure 5 and parameters are in Table 1. This functional form of specific heat was integrated over temperature to determine the enthalpy of solid RDX using the value at 298 K to obtain the integration constant. This treatment differs from that of Liao and Yang [2] and Liao [9] in that their model assumes a constant value of specific heat.

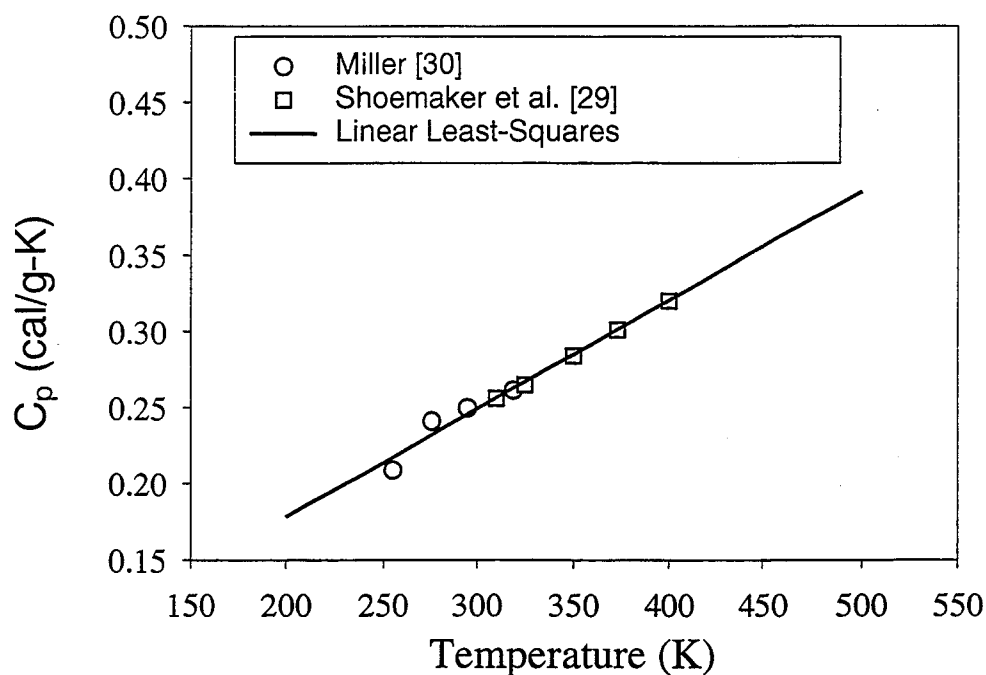


**Figure 5. Specific Heat of RDX.**

Finally, the detailed reaction mechanism occurring in the gas phase needs to be specified, along with the associated thermodynamic and transport parameters. The reaction mechanism, thermodynamic data, and transport adopted here are the same as those used by Liao and

**Table 1. Semi-Empirical Model Parameters**

As (cm/s)	$E_s/R$ (K)	$\rho_s$ (g/cm <sup>3</sup> )	$C_p$ (cal/g-K)	$H_{RDX}$ (cal/mol)
$3/695 \times 10^5$	9,330	1.66 <sup>a</sup>	$0.03604 + 7.105 \times 10^{-4} T$	14,690 at 298 K

<sup>a</sup>This value was reported by Zenin [7] for his pressed specimens.

Yang [2] and Liao [9]. In both models, the gas-phase conservation equations are solved using adaptations of the PREMIX code [31] developed at Sandia National Laboratories.

Some discussion of the difference between the two models is in order. The Liao and Yang model [2, 9] is a more fundamental treatment than the semi-empirical model, in the sense that the regression mechanism is treated explicitly. This mechanism is mostly evaporative, with some small part due to RDX condensed-phase reactions. It is also more fundamental because it does not rely on measurements made at every pressure for which a calculated burning rate is desired. The semi-empirical model requires a measurement of surface temperatures at all pressures, and these measurements are known to fail at sufficiently high pressures due to thermocouple response errors. The condensed-phase reactions and the evaporation description (to some degree) are uncertain, however, and these uncertainties map into the model results in an unknown way. Our semi-empirical model, on the other hand, at the expense of giving less detail about the condensed phase (e.g., liquid-layer thickness), compensates empirically for these uncertainties in underlying fundamentals. Hence, it may provide a better test of the gas-phase reaction mechanism. This is true, at least to the extent that the surface temperature data is accurate, and our assumption of no condensed-phase reactions is warranted. In any event, Figure 6 shows that the major species profiles computed by the two models, as well as the temperature profiles, do not differ to any significant degree. It can be inferred from this agreement that the Liao and Yang description of the condensed-phase and surface-regression mechanism is in substantial agreement with the net physical effects of the condensed-phase processes, as expressed by the experimentally calibrated pyrolysis law. However, it is also true that since the condensed-phase reactions appeared to play a small role in the RDX combustion, the detailed description of the condensed-phase processes was not stringently tested. For

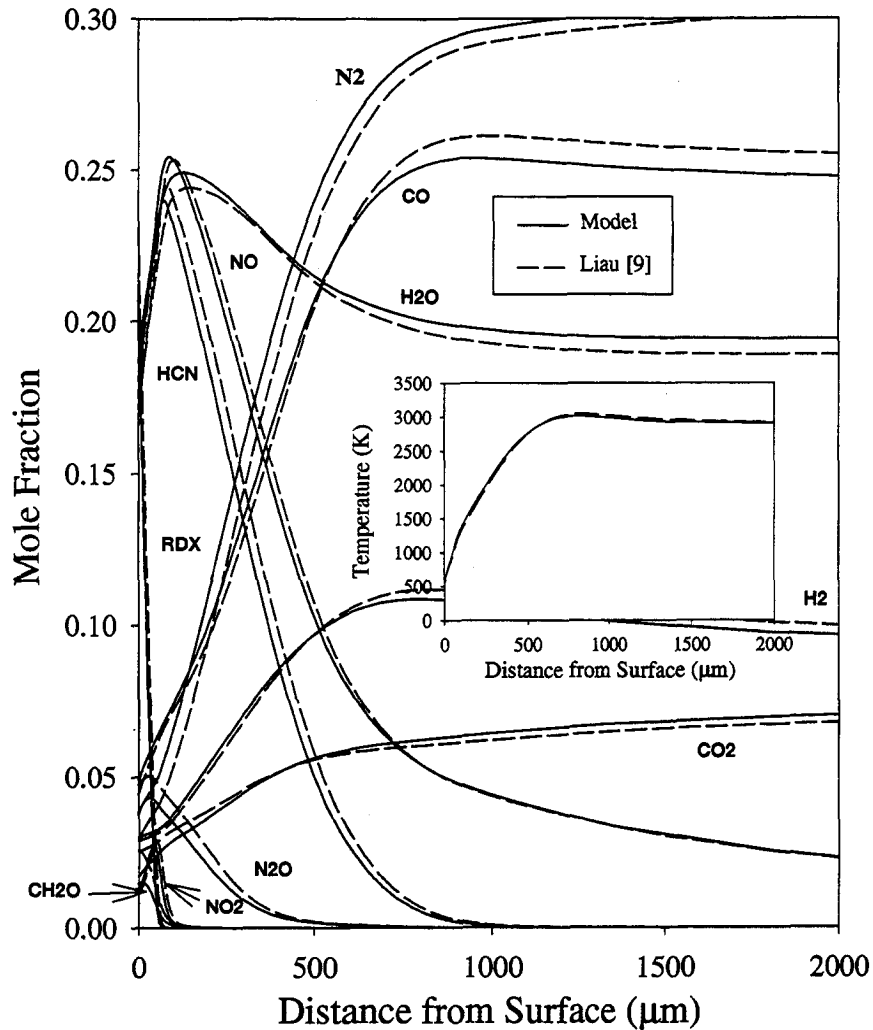


**Figure 6. RDX Species Model Profiles.**

purposes of comparison, it is reassuring that the results from such different condensed-phase treatments are so close.

There is an important discrepancy between one of the assumptions of this model and an inference made by Zenin [7] based on his microthermocouple data. We believe that all of the RDX models [1–4] are similarly discrepant. Zenin found that the net enthalpy change at the surface decreased monotonically with increasing pressure. This enthalpy change was computed to be +84 cal/g at 1 atm, +61 cal/g at 5 atm, -58 cal/g at 20 atm, and -140 cal/g at 90 atm. Positive enthalpy changes are consistent with an endothermic process such as evaporation, but

negative enthalpy changes are not. Thus, the possibility exists that the good agreement between models and experimental burning rates shown later in Figure 17 is merely fortuitous. Zenin's inference [7] that the surface enthalpy change decreases with increasing pressure depends on the accuracy of both the measured surface temperature and the numerical derivative of the temperature at the surface. These are notoriously difficult measurements, and Zenin [7] gave no analysis or discussion of experimental uncertainties. Therefore, there was no way to determine how sensitive the validity of the inference was to the experimental uncertainties. At this time, there appears to be no way to resolve this issue, but future work should be directed toward understanding this inconsistency.

## 5. Results

**5.1 Absorption.** In Figure 7, OH concentration profiles in 1-atm air measured with the snapshot technique are compared to experimental values obtained by Parr and Hanson-Parr [15] and Ulas et al. [16]. Our model predictions and those of Liao and Yang [2] and Liao [9] and Melius and Yetter in Liao [9] are also presented in this figure. Parr's values were obtained by absorption spectroscopy-calibrated planar-laser-induced fluorescence of RDX in 1-atm air. Attempts to conduct self-deflagration measurements in 1-atm nitrogen were unsuccessful, confirming observations by Ulas et al. [16] who conducted their experiments at 1.7 atm. At distances greater than 2 mm from the surface (well into the luminous flame zone), the measured concentration of OH approaches the adiabatic value of 0.024-mol fraction (MF), as calculated using the NASA-Lewis thermochemical code. OH species concentrations also approach the adiabatic values for 2-atm air, as shown in Figure 8. In this case, the concentration reaches a steady-state value closer to the surface. This is supported by visual evidence that the offset of the luminous flame zone decreases with higher pressure. The quantity of OH and its vibrational structure is very sensitive to temperature. As the temperature decreases toward the surface, the amount of OH is significantly reduced. This results in degraded signal-to-noise ratios, thus yielding unreliable temperatures. Because of the difficulty of obtaining precise measurements directly from the CN and NH spectra, temperature profiles were obtained by combining our measured OH temperatures in the flame with OH and thermocouple (TC) values from the

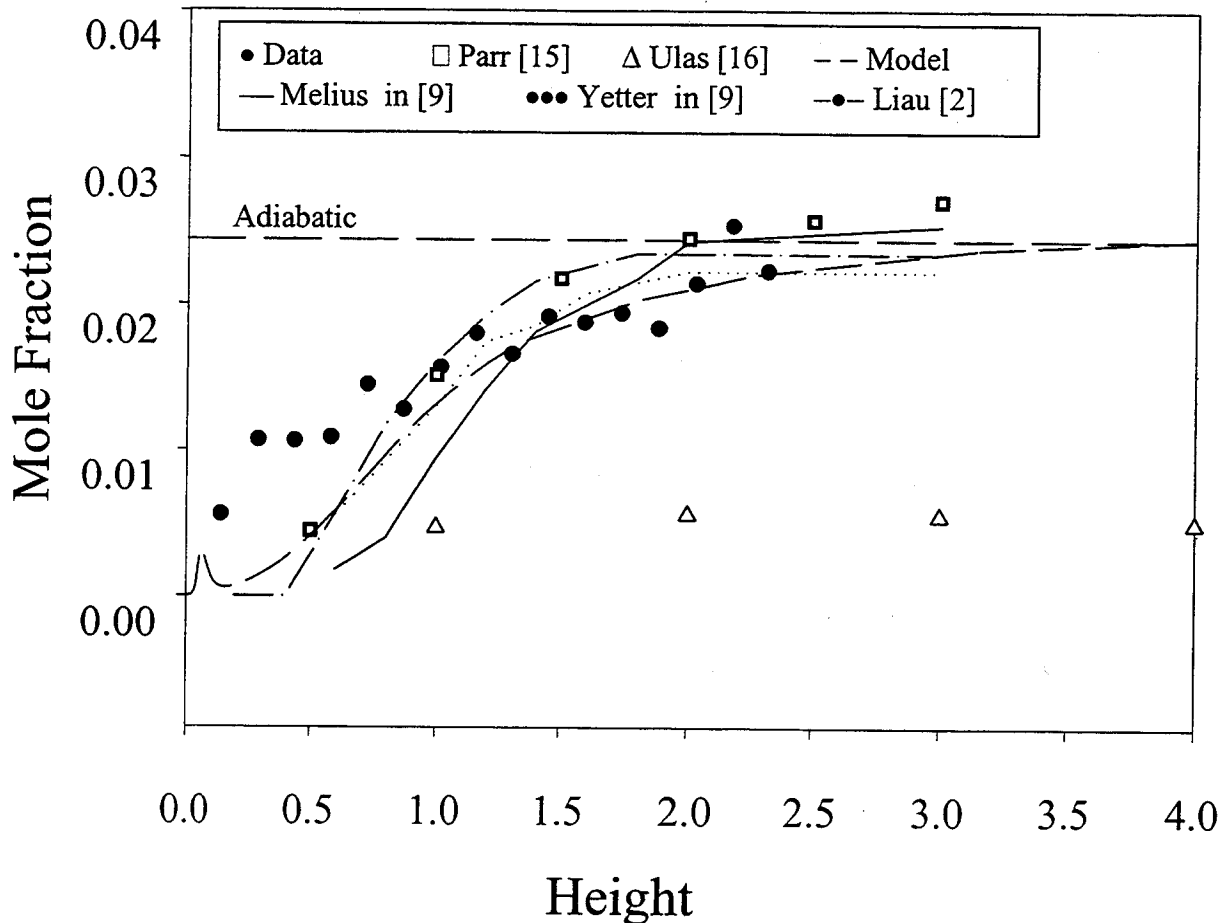


**Figure 7. OH Concentration Profile at 1 atm.**

literature. Data from Zenin [7] and Hanson-Parr and Parr [12] at 1 atm, combined with temperature data from OH spectra, are shown in Figure 9. At higher pressures, the OH concentrations (and temperature) near the propellant surface are increased, thereby allowing for a more reliable temperature fit. Temperatures obtained from OH spectra at 2 atm are shown in Figure 10. At this point, it was assumed that the temperature profile for 1.5 atm fell midway between the 1- and 2-atm profiles. The temperature was therefore removed as a variable from the multivariate fits for NH and CN.

Figure 11 shows a spectrum indicating CN absorption from the  $B^2\Sigma^+ - X^2\Sigma^+$  system around 386 nm, together with the accompanying fits. This snapshot spectrum was taken 0.7 mm from

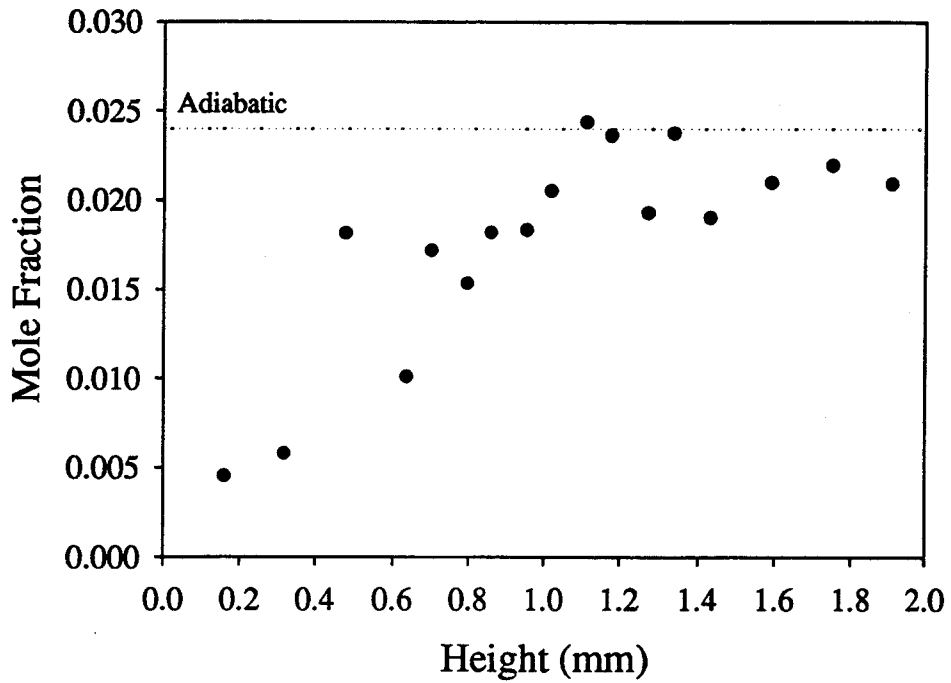


Figure 8. OH Concentration Profile at 2 atm.

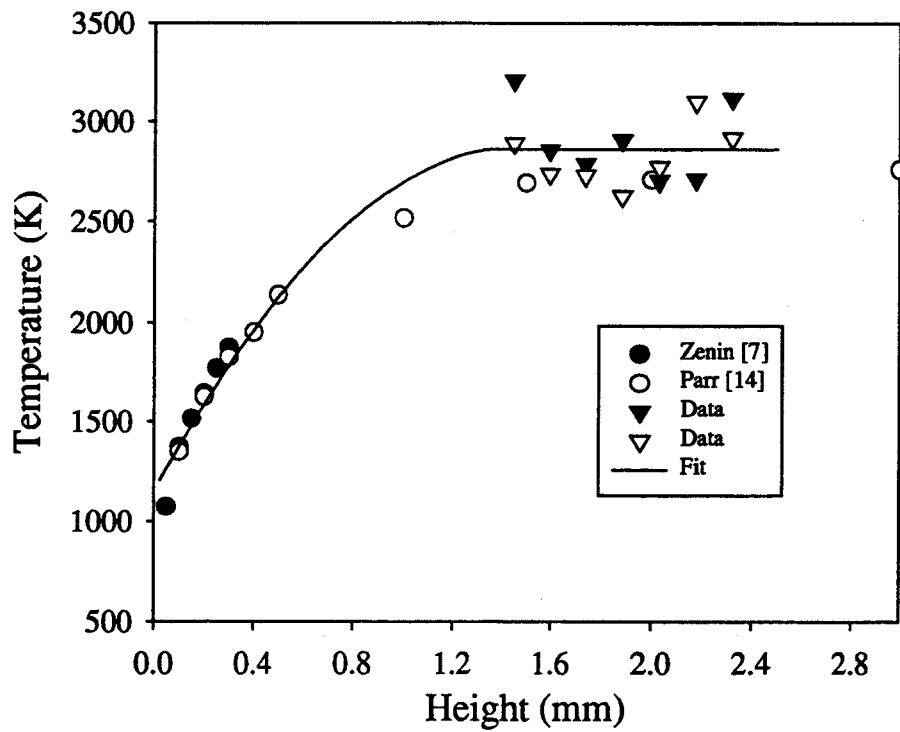


Figure 9. 1-atm Temperature Profile for RDX.

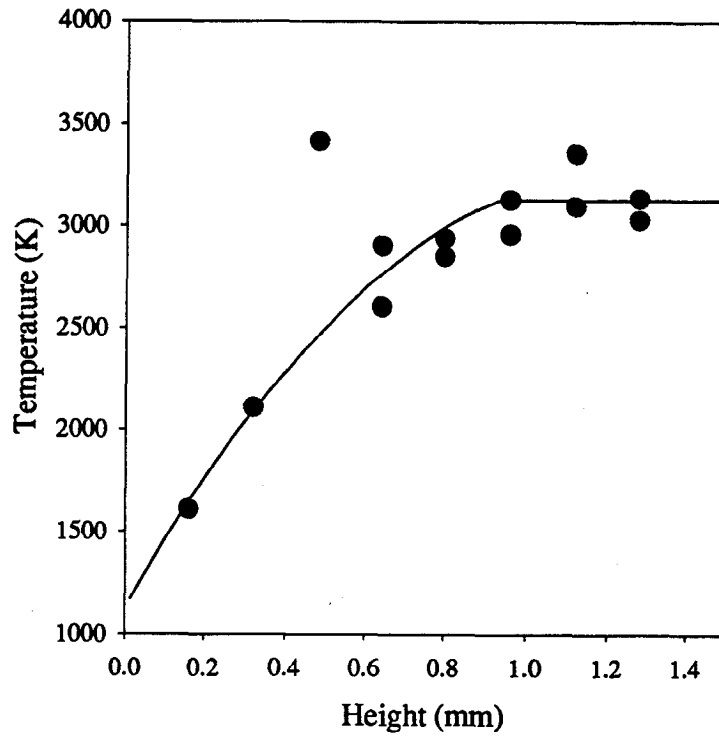


Figure 10. 2-atm Temperature Profile Obtained From OH Spectra.

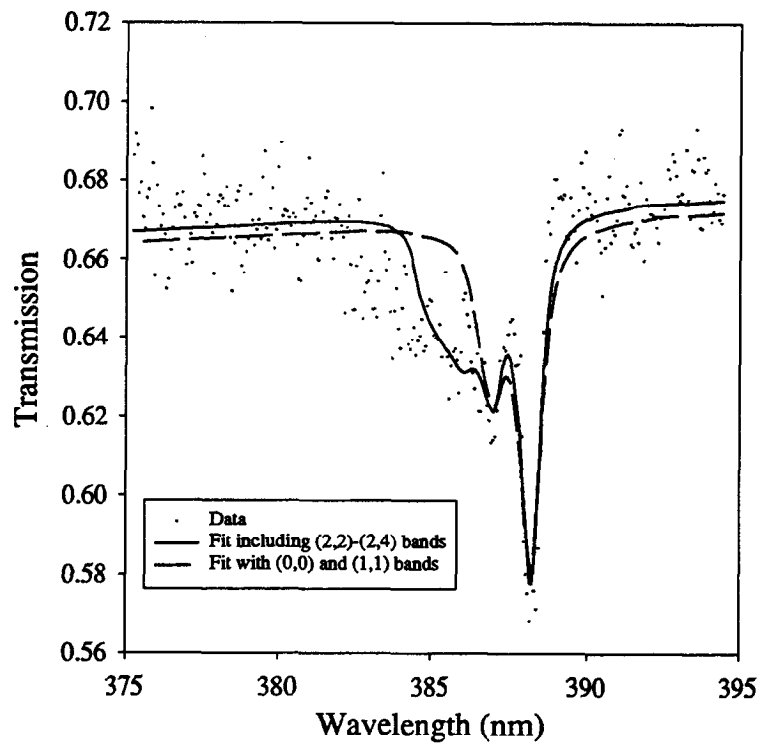
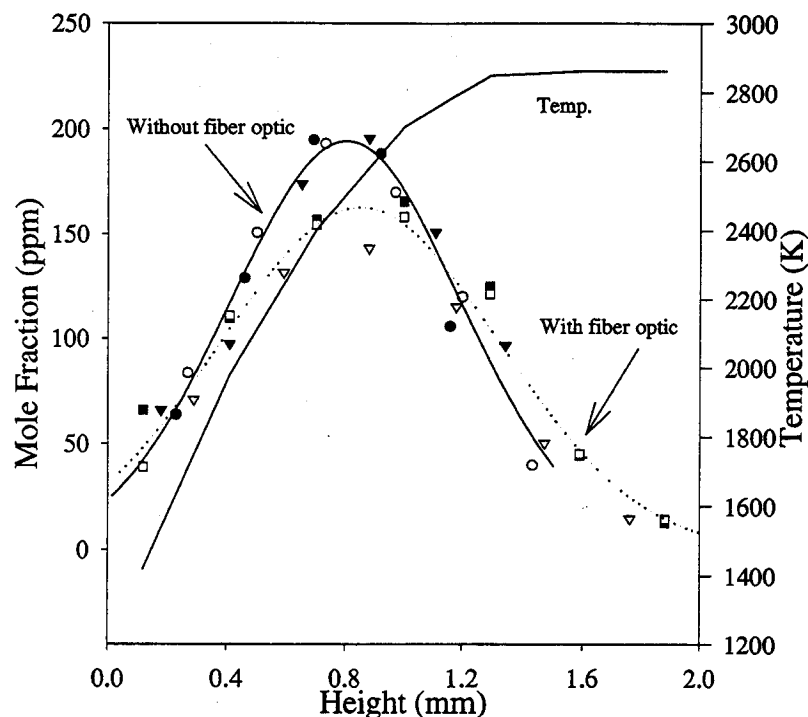


Figure 11. CN Spectrum for 1 atm, 0.7 mm From Sample Surface.

the surface of RDX while it was undergoing self-sustained combustion in 1-atm air. The dashed line represents a fit where only the (0,0) and (1,1) vibrational transitions are included. Including the (2,2)–(4,4) bands (solid line) significantly improved the fit to the data. Although a narrower instrument resolution would seem warranted for this figure, results from the more reliable calibration technique that uses a low-pressure pen lamp were used to fix this parameter. The solid line fit to the data results in a CN mole fraction of 175 ppm. According to the procedure described previously to determine the path length, an 11% correction to this data resulted in a CN mole fraction value of 195 ppm.

Figure 12 shows three CN mole fraction profile snapshots in 1-atm air for two different RDX combustion runs. In addition, Gaussian functions are plotted as a simple representation of the two data sets. For reference, the temperature profile for 1-atm RDX combustion in air is also plotted on the same graph. Within experimental uncertainty, a Gaussian adequately represents the experimental data. For one of the runs, a fiber optic was substituted for the collection lens in an attempt to determine possible effects of beam steering on the CN concentration profile. The propellant sample was positioned to initially cover some of the measurement strips. Therefore, the zero of the height scale (or distance from the propellant surface) was determined by the onset of the transmission signal balanced against visual evidence from the video camera. Only small differences occur in both maximum CN concentration and the position of maximum CN concentration. These differences are well within the uncertainty associated with run-to-run variations and demonstrate that beam steering is not compromising the data at this level of spatial resolution.

Snapshot CN profiles of RDX combustion were also conducted at higher pressures. In 1.5-atm air, the position of maximum CN concentration decreased from ~0.82 mm (1 atm) to 0.59 mm, and the FWHM width also decreased from 1.1 mm (1 atm) to 0.78 mm. A decrease in the maximum CN mole fraction was also observed. The width was again 0.78 mm for the 2-atm case. However, the position of maximum CN concentration increased to 0.71 mm, while the



**Figure 12. CN Concentration Profile at 1 atm.**

maximum CN mole fraction decreased by about a factor of two. Here, the data were more scattered, and a Gaussian-like shape was not well defined.

Snapshot NH concentration fraction profiles for RDX combustion in 1-atm air are shown in Figure 13. There was considerably more scatter in the data due to the reduction in S/N, inherent for NH measurements. Hence, a Gaussian-function representation of this data was only applied for consistency. The determined position of a maximum NH mole fraction (0.81 mm) was the same as that for CN (0.82 mm) at 1-atm air pressure.

Snapshot profiles of CN and NH were also conducted at higher pressures and are summarized in Table 2. The position and widths of the concentration profiles generally decreased above atmospheric pressure, as would be expected from the visual evidence. Due to the limited spatial resolution of this technique, both peak positions and widths became less certain as the pressure was increased to 2 atm. For both CN and NH, there is a monotonic decrease in the measured concentration with increased pressure.

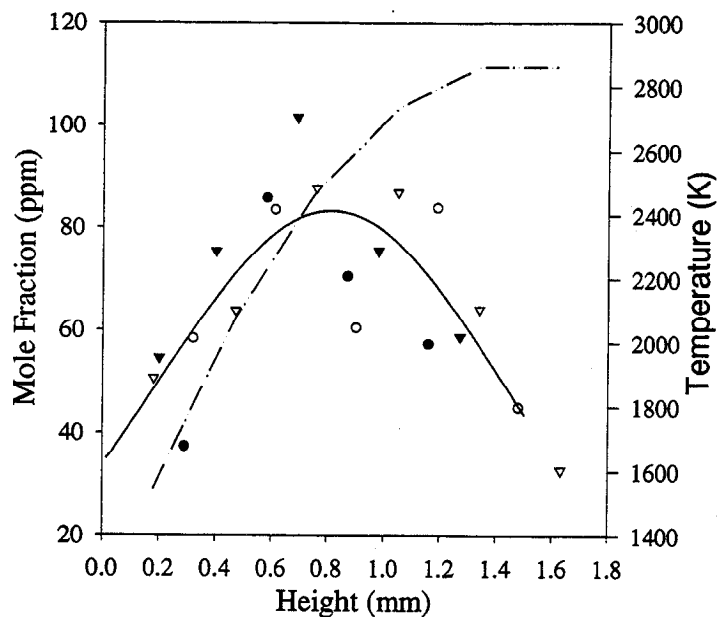
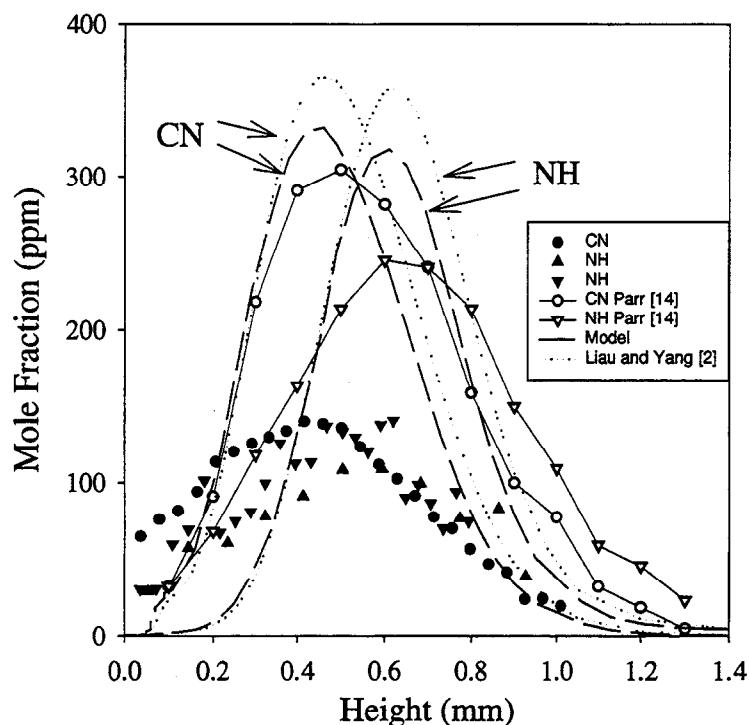


Figure 13. NH Profiles in 1-atm Air.

Table 2. Comparison of CN and NH Concentrations Obtained in the Self-Sustained Combustion of RDX

Molecule	Pressure (atm)	Peak Concentration (ppm)	FWHM (mm)	Peak Standoff (mm)	Author
CN	1	160-190	1.1	0.85	Present work, snapshot
CN	1	140	0.70	0.4	Present work, high resolution
CN	1	310	0.6	0.5	Parr and Hanson-Parr [14]
CN	1	375	0.42	0.49	Liau and Yang [2] (model)
CN	1	340	0.40	0.47	Present work (model)
CN	1.5	140	0.8	0.6	Present work, snapshot
CN	2	80	0.8	0.7	Present work, snapshot
NH	1	80	1.4	0.8	Present work, snapshot
NH	1	120	0.7	0.5	Present work, high resolution
NH	1	260	0.65	0.6	Parr and Hanson-Parr [14]
NH	1	360	0.38	0.63	Liau and Yang [2] (model)
NH	1	245	0.65	0.64	Present work, (model)
NH	1.5	70	1.0	0.6	Present work, snapshot
NH	2	60	1.2	0.5	Present work, snapshot

Higher resolution 1-atm CN and NH concentration profiles (Figure 14) were obtained with the single-beam absorption experimental setup. Spatial information was gathered in this case by allowing the sample to burn by the probe beam. The measured concentration peak position and model for both CN and NH agree well with values measured by Parr and Hanson-Parr [14] and predicted by Liao and Yang [2] and Liao [9]. Although our measured species mole fraction compared to within a factor of two, the ratio of CN to NH of  $\sim 1.2$  was consistent.



**Figure 14. High Resolution Profiles of CN and NH at 1 atm.**

The NO species concentration profile of burning RDX in 1-atm air is compared to data from Parr and Hanson-Parr [14] in Figure 15. In this case, the Parrs used absorption spectroscopy due to the large self-absorption that adversely effects LIF measurements of this species. Current modeling results and predictions from Liao and Yang [2] and Liao [9] also appear in this figure. Data was taken by conventional single beam absorption spectroscopy because of the greater spatial resolution afforded this technique. At distances greater than 0.5 mm from the surface,

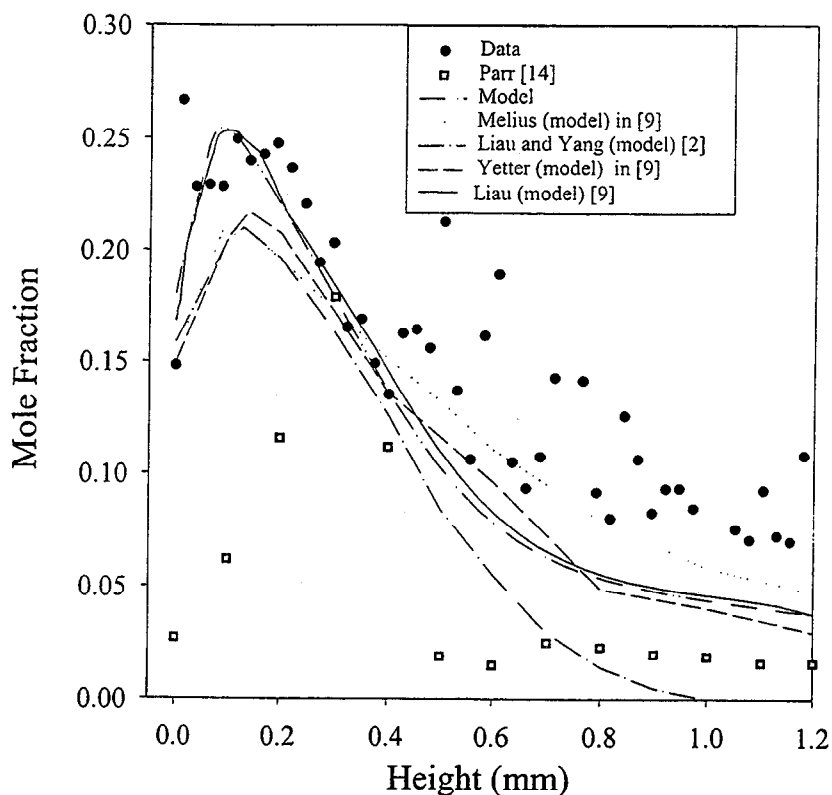


**Figure 15. High Resolution NO Species Profiles.**

well into the final flame zone, measured species concentrations were higher than those predicted by the models. In the same region, the temperature of NO (Figure 16) is less than that measured by the OH diagnostic or predicted by the models. This higher concentration is most likely caused by the presence of cold NO molecules lying in the absorption path, but outside of the flame region. This effect becomes prevalent as the sample deflagrates due to the sequential spectra collection scheme, with early (closer to the surface) measurements being least affected.

**5.2 Video Records.** In addition to the information obtained from analysis of absorption spectra, a video record exists for each experiment. A typical video frame for RDX combustion is shown in Figure 3. Both burning rates and flame structure have been determined from these video records. Table 3 contains distance estimates for the dark zone and the CN reaction zone lengths. These distance estimates come from visible light emission, as seen by the Cohu CCD color camera. The thickness of the violet-colored region above the combusting RDX surface is taken as the FWHM thickness for the CN concentration. The nonluminous region between the

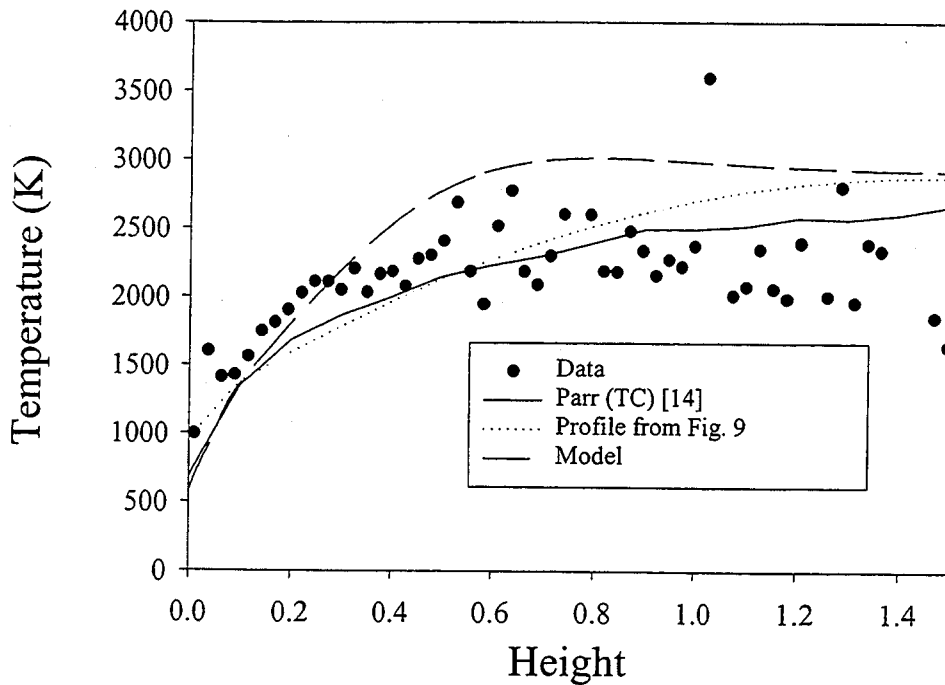


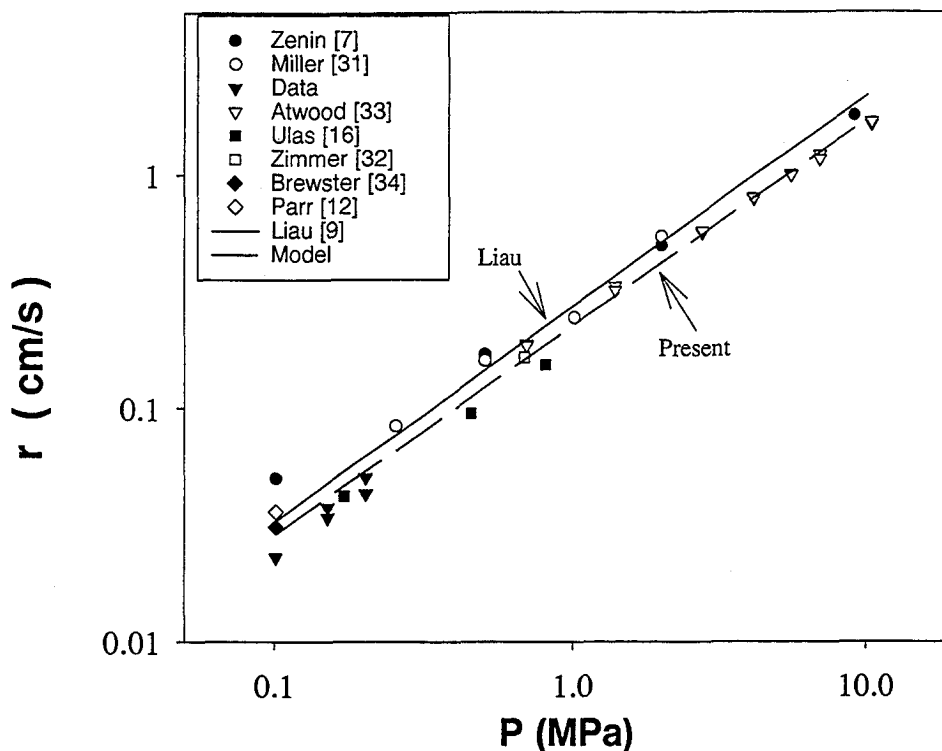
Figure 16. Temperature Profile From NO Spectra at 1 atm.

Table 3. Video Measurements for RDX Burning in Air

Pressure (atm)	Dark Zone Length (mm)	CN Reaction Zone Length (mm) (~FWHM)
1.0	0.3	0.5
1.5	0.2	0.3
2.0	0.1	0.2

RDX combusting surface and the start of the violet region is taken as the measure of the dark zone. These values were compared with absorption data and other published work in the discussion section.

**5.3 Burning Rate.** In Figure 17, the results of the two model calculations of burning rate are compared to a number of sets of experimental rate measurements. Both models agree well with the data. Liau and Yang [2] and Liau [9] noted that over the pressure range displayed, the endothermic condensed-phase reaction dominated the exothermic reaction, and did so to a



**Figure 17. Burn Rate of RDX as a Function of Pressure.**

greater extent at the lower pressure. This may explain the slightly higher pressure exponent evident with that model.

Burning rates as a function of pressure are given in Figure 17. Other published measurements are also plotted on the same figure for comparison. Measurements of Zenin [7], Ulas et al. [16], Zimmer-Galler [32], and Atwood et al. [33] use nitrogen as the pressurizing gas. Brewster and Schroeder's [34] results, Parr and Hanson-Parr's [14] results, and the present results are measurements for an air environment. The burning rate for RDX combusting in 2-atm nitrogen gas was also measured. Well within experimental uncertainty, we found the burning rates for the air and nitrogen environments to be the same, even though the gas-phase structure appears different close to the edges where air can be entrained into the combustion process. A more pronounced rounding of the edges is attributed to this entrainment. Experimental burning rate measurements for RDX vary by a factor of two at atmospheric pressure, and our result of 0.23 mm/s represents the lowest value. Zenin's values are the highest. These present measurements at atmospheric pressure, within experimental uncertainty, agree with Brewster and

Schroeder [34] and Parr and Hanson-Parr [14]. Our burning rate values for 1.0, 1.5, and 2.0 atm, line up best with the results of Ulas et al. [16]. A video observation of the RDX combustion shows that convex surfaces can occur, especially for the smaller diameter samples. Moreover, small and large bubbles form in the melt layer, giving rise to occasional surface movement being driven by buoyant effects. Sample preparation, impurities, and density can also effect the measured burning rate of the propellant.

## 6. Discussion

Measurements of the highly reactive intermediate species, CN and NH, require a high degree of spatial resolution, as these species are formed and consumed over a small spatial extent. Furthermore, this spatial extent is pressure dependent, decreasing as the pressure increases. Consequently, the maximum spatial resolution for a line-of-sight technique (absorption) is severely challenged when applied to making measurements across a burning, moving propellant surface. Any nonplanar burning and/or misalignments of the absorption light beam with the thin region, where short-lived radical species exist, leads to degradation of the apparent spatial resolution. A quick calculation shows an 18% drop in apparent concentration for CN, and NH is possible with as little as five degrees of misalignment. The harsh reality that the combustion of propellants does not produce ideal, 1-D systems, is indeed a concern that current models and absorption spectroscopy techniques ignore. However, much effort has been expended to produce a large area on the top of the sample that is flat to within the resolution of the visual record ( $<100\ \mu\text{m}$ ). There is a small region on the edge of the combustion zone that is not in line with this flat region but follows the curved edge of the sample. If the combustion wave follows the topography of the sample, the line-of-sight path length in this curved region is on the order of the spatial extent of the species being measured. Because of the narrow profiles of NO, CN, and NH, the absorption path length in this outside region of the combustion zone is small compared to that over the flat portion. Furthermore, convolution of the finite absorption beam diameter (assumed circular) with the calculated species profiles (assumed Gaussian) produced only small effects in the final profile ( $<5\%$ ). Unfortunately, there must be an assumption made about the shape of the actual profile to deconvolute the experimental data. For the reasons already

mentioned, the best results should be for RDX burning in 1-atm air (the lowest pressure data, where the spatial resolution requirements are the least stringent). A comparison with other published results for 1-atm conditions are discussed, followed by an interpretation of the higher pressure data.

Table 2 provides a summary of the CN and NH peak concentrations, widths of the species profile, and peak standoff distances obtained for self-sustained RDX combustion at pressures ranging from 1 to 2 atm air. For a comparison, the Parrs' are the only known investigators who have published quantitative results for species concentrations in the self-deflagration of RDX at 1-atm air pressure. In their more recent measurements, Parr and Hanson-Parr [14] report peak CN mole fractions of 310 ppm for self-sustained combustion of RDX in 1-atm air. These measurements were made for 9.5-mm diameter pressed RDX propellant samples. In this same work, they report peak NH mole fractions of 260 ppm. Looking at column four of Table 2, which is a measure of the spatial extent of the profiles, in all cases the Parr data gives a smaller spatial extent (by about a factor of two) than our measurements taken with the snapshot technique. However, data from the high-resolution experiment more closely matches the position and widths of these two species. It should be noted that the video estimates (Table 3) of the FWHM values also support the high-resolution data.

As the measured concentration profile and models of NO reach a maximum close to the surface, the peak position and the height from this peak to half max (HM) provides an indication of the extent of NO and is reported in Table 4. Our measurements of substantial NO at the surface (0.15 MF) agree well with the predictions of the models. In contrast, Parr and Hanson-Parr [14] measured very little NO at the surface, with the peak concentration occurring a factor of two further into the dark zone.

As far as the pressure dependence of the CN and NH profiles taken with the snapshot technique, the behavior suggests a spatial resolution limitation at the elevated pressures. The peak standoff distance, as well as the extent (FWHM) of the profile, is expected to decrease

**Table 4. Comparison of NO Concentrations at 1-atm Air**

Peak Concentration	Peak Standoff (mm)	Half-Max Standoff From Peak Position (mm)	Author
0.25	0.1	0.4	Present work, high resolution
0.17	0.4	0.1	Parr and Hanson-Parr [14]
0.26	0.09	0.33	Present work (model)
0.21	0.13	0.34	Liau and Yang [2] (model)

with increasing pressure. Only a slight indication of this trend is present from the absorption data of Table 2, while estimates from video records (Table 3) suggest more pronounced decreases in peak standoff and FWHM with increasing pressure. For propellant diagnostics of small samples with short temporal constraints, or samples with large reaction zones and reduced spatial needs, the snapshot absorption technique is useful.

Species profiles in RDX flames have been obtained during 1-atm self-deflagrating combustion. Although the peak concentrations of CN and NH differ by a factor of two, both the model and other researcher's measurements [14] and the positions and concentration ratio measured by the high-resolution technique are very close. The factor of two difference in concentration is not alarming, as CN and NH are minor concentration species existing in a small region close to the combusting surface. Because NO is a major species both in concentration and importance to the combustion process, the differences between the profiles measured in this work and that of Parr and Hanson-Parr [14] for the same combustion conditions are more of a concern. Parr and Hanson-Parr [14] used a military grade of RDX that contained up to 5% HMX (assayed), whereas our samples were recrystallized to remove such impurities. Some of the difference in concentration measured at the surface may be due to this impurity since it is thought that HMX produces less NO at the surface. The choice of absorption path length will also effect the measured concentration. In this work, the path length was chosen to coincide with the visual extent of the CN region (see Figure 3). Parr and Hanson-Parr [14] chose a longer path,

which was determined by the presence of a brown gas ( $\text{NO}_2$ ) with a diameter larger than the propellant. This brown gas was not apparent in our measurements. Further evidence of the high concentration of NO near the surface came from recent measurements of Hanson-Parr and Parr [35] using spontaneous Raman spectroscopy as the diagnostic tool. Their measured value of 0.26 MF NO within 0.1 mm of the surface is in good agreement with our measured and predicted values.

Current model predictions are in good agreement with the concentration profiles for all four species measured in this work. The gas-phase mechanism used to model RDX combustion has been able to predict species profiles under various experimental conditions [2, 4, 9]. However, evaporation from the surface, RDX subsurface decomposition mechanisms, and thermophysical properties of the liquid layer are all avenues for further research.

## 7. Conclusions

RDX has become the principal prototype in the study of the detailed combustion mechanisms of energetic materials. Experimental verification of these mechanisms is, therefore, of central interest to this research. The combined experimental and modeling efforts presented in this report are an attempt to clarify and extend the limits of the present understanding.

Calculations of the burning rate are the result of integration over the fundamental chemical and physical mechanisms; for this reason, successful model predictions of the measured burning rates are not a particularly sensitive test of the validity of model assumptions. A more stringent test is afforded by comparing model and experimental species profiles. In this work, new measurements are presented for four gas-phase species profiles, OH, NO, CN, and NH, arising from the steady-state combustion of RDX at pressures of 1–2 atm. Under these same conditions, there has been only one other group to measure the species profiled in this report. In that effort [12–14], diagnostic techniques different from those used in this work were applied to the measurement of the OH, CN, and NH species, and more recently NO [35]. The independent and complementary nature of these two sets of measurements are important in building a reliable

experimental database with which to test the models. The two sets of measurements are generally consistent with differences detailed in the discussion section.

The experimental species profiles are compared with predictions of two models of RDX combustion that attempt to follow the elementary gas-phase reactions in detail. Like the two sets of experimental measurements, these two models are somewhat complementary in that they both use the same gas-phase reaction mechanism, but treat the condensed-phase and surface gasification mechanism differently. One model was previously developed by Liao and Yang [2] and Liao [9], and the other is presented in this report. Due to the new model's use of an empirical relationship between burning rate and surface temperature (pyrolysis law), it is less speculative of the condensed-phase processes. But the Liao and Yang model gives a more detailed description of the condensed-phase processes. Because the two models predict virtually the same burning rates and species profiles, despite their differing treatments of the condensed-phase processes, comparisons between experimental and theoretical profiles in the gas phase should be a meaningful test of the reaction mechanism there. Agreement between our new species profiles and the corresponding model predictions are judged to be within our experimental uncertainty. This favorable comparison, coupled with the good agreement between measured and predicted burning rates, adds considerable confidence to the validity of the gas-phase reaction mechanism.

INTENTIONALLY LEFT BLANK.

## 8. References

1. Melius, C. F. "The Gas-Phase Flame Chemistry of Nitramine Combustion." *Proceedings of the 25th JANNAF Combustion Meeting*, CPIA Publication 498, vol. 2, pp. 155–162, 1988.
2. Liao, Y. C., and V. Yang. "Analysis of RDX Monopropellant Combustion With Two-Phase Subsurface Reactions." *Journal of Propulsion and Power*, vol. 11, no. 4, pp. 729–739, 1995.
3. Li, S. C., and F. A. Williams. "Nitramine Deflagration: Reduced Chemical Mechanism for Primary Flame Facilitating Simplified Asymptotic Analysis." *Journal of Propulsion and Power*, vol. 12, no. 2, pp. 302–309, 1996.
4. Davidson, J. M., and M. Beckstead. "Improvements to RDX Combustion Modeling." *American Institute of Aeronautics and Astronautics*, AIAA 96-0885, pp. 1–11, 1996.
5. Ermolin, N. E., O. P. Korobeinichev, L. V. Kuibida, and V. M. Fomin. "Study of the Kinetics and Mechanism of Chemical Reactions in Hexogen Flames." *Fizika Goreniya i Vzryva*, vol. 22, no. 5, pp. 544–553, 1986.
6. Hatch, R. L. "Chemical Kinetics Modeling of HMX Combustion." *Proceedings of the 24th JANNAF Combustion Meeting*, CPIA Publication 476, vol. 1, pp. 383–391, 1987.
7. Zenin, A. "HMX and RDX: Combustion Mechanism and Influence on Modern Double-Base Propellant Combustion." *Journal of Propulsion and Power*, vol. 11, no. 4, pp. 752–758, 1995.
8. Brill, T. B. "Multiphase Chemistry Considerations at the Surface of Burning Nitramine Monopropellants." *Journal of Propulsion and Power*, vol. 11, no. 4, pp. 740–751, 1995.
9. Liao, Y. C. "A Comprehensive Analysis of RDX Propellant Combustion and Ignition With Two-Phase Subsurface Reactions." Ph.D. dissertation, Pennsylvania State University, Dept. of Mechanical Engineering, May 1997.
10. Korobeinichev, O. P. "Dynamic Flame Probe Mass Spectrometry and Condensed System Decomposition." *Fizika Goreniya i Vzryva*, vol. 23, no. 5, pp. 64–76, 1987.
11. Litzinger, T. A., B. L. Fetherolf, Y. J. Lee, and C. J. Tang. "A Study of the Gas-Phase Chemistry of RDX: Experiments and Modeling." *Journal of Propulsion and Power*, vol. 11, no. 4, pp. 698–703, 1995.
12. Hanson-Parr, D., and T. Parr. "RDX Flame Structure." *Proceedings of the Twenty-Fifth Symposium (Int.) on Combustion*, The Combustion Institute, pp. 1635–1643, 1994.

13. Parr, T., and D. Hanson-Parr. "RDX, HMX, and XM39 Self-Deflagration Flame Structure." *Proceedings of the 32nd JANNAF Combustion Meeting*, CPIA Publication 631, vol. 1, pp. 429-437, 1995.
14. Parr, T., and D. Hanson-Parr. "Solid Propellant Flame Structure." *Decomposition, Combustion and Detonation Chemistry of Energetic Materials*, edited by T. B. Brill, T. P. Russell, W. C. Tao, and R. B. Wade, Mater. Res. Soc. Proc. 418, Pittsburgh, PA, pp. 207-219, 1995.
15. Parr, T., and D. Hanson-Parr. Personal communication with B. Homan. 1998.
16. Ulas, A., Y. C. Lu, K. K. Kuo, and T. Freyman. "Measurement of Temperature and NO and OH Concentrations of Solid Propellant Flames Using Absorption Spectroscopy." *Proceedings of the 32nd JANNAF Combustion Meeting*, CPIA Publication 631, vol. I, pp. 461-469, 1995.
17. Vanderhoff, J. A. "Spectral Studies of Solid Propellant Combustion II. Emission and Absorption Results for M-30 and HMX1 Propellants." BRL-TR-3055, U.S. Army Ballistic Research Laboratory, Aberdeen Proving Ground, MD, December 1989.
18. Vanderhoff, J. A. "Species Profiles in Solid Propellant Flames Using Absorption and Emission Spectroscopy." *Combustion and Flame*, vol. 84, pp. 73-92, 1991.
19. Vanderhoff, J. A., M. W. Teague, and A. J. Kotlar. "Determination of Temperature and NO Concentrations Through the Dark Zone of Solid-Propellant Flames." *Proceedings of the Twenty-Fourth Symposium (International) on Combustion*, The Combustion Institute, Pittsburgh, PA, pp. 15-1922, 1992.
20. Modiano, S. H., and J. A. Vanderhoff. "Propellant Dark Zone Concentrations via Multichannel IR Absorption." *Proceedings of the Twenty-Sixth Symposium (International) on Combustion*, The Combustion Institute, Pittsburgh, PA, vol. 2, pp. 2017-2023, 1996.
21. Modiano, S. H., and J. A. Vanderhoff. "Multichannel Infrared (IR) Absorption Spectroscopy Applied to Solid Propellant Flames." ARL-TR-900, U.S. Army Research Laboratory, Aberdeen Proving Ground, MD, December 1995.
22. Homan, B. E., and J. A. Vanderhoff. "Snapshot Absorption Spectroscopy." *Applied Spectroscopy*, vol. 53, pp. 816-821, 1999.
23. Weinberg, F. J. *Optics of Flames*. Washington, DC: Butterworth, 1963.
24. Vanderhoff, J. A., M. W. Teague, and A. J. Kotlar. "Determination of Temperature and NO Concentrations Through the Dark Zone of Solid Propellant Flames." *Proceedings of the 24th Symposium (International) on Combustion*, The Combustion Institute, pp. 1915-1922, 1992.

25. Suchard, S. N., ed. *Spectroscopic Data Heteronuclear Diatomic Molecules, Part A*. New York:IFI/Plenum Publishing, vol. 1, p. 291, 1975.
26. Miller, M. S., and W. R. Anderson. "Energetic-Material Combustion Modeling With Elementary Gas-Phase Reactions: A Practical Approach," in "Solid Propellant Combustion Chemistry, Combustion, and Motor Interior Ballistics." V. Yang, T. Brill, and W. Ren, eds., *AIAA*, vol. 185, pp. 501–531, 2000.
27. Lengelle, G. "Thermal Degradation Kinetics and Surface Pyrolysis of Vinyl Polymers." *AIAA Journal*, vol. 8, pp. 1989–1996, 1970.
28. Zenin, A. A. "Thermophysics of Stable Combustion Waves of Solid Propellants in Nonsteady Burning and Combustion Stability of Solid Propellants." Edited by L. DeLuca, E. W. Price, and M. Summerfield, *Progress in Astronautics and Aeronautics*, AIAA, Washington, DC, vol. 143, pp. 197–231, 1992.
29. Shoemaker, R. L., J. A. Stark, and R. E. Taylor. "Thermophysical Properties of Propellants." *High Temperatures – High Pressures*, vol. 17, pp. 429–435, 1985.
30. Miller, M. S. *Journal of Thermophysics and Heat Transfer*. Vol. 8, pp. 803–805, 1994.
31. Kee, R. J., J. F. Grcar, M. D. Smooke, and J. A. Miller. "A Fortran Program for Modeling Steady Laminar One-Dimensional Premixed Flames." SAND85-8240, Sandia National Laboratories, 1991.
32. Zimmer-Galler, R. "Correlations Between Deflagration Characteristics and Surface Properties of Nitramine-Based Propellants." *AIAA Journal*, vol. 6, no. 11, pp. 2107–2110, 1968.
33. Atwood, A., P. O. Curran, C. F. Price, and J. Wiknich. "Burning Rate, Radiant Ignition, and Global Kinetics of Cyclotrimethylene Trinitramine (RDX)." *Proceedings of the 32nd JANNAF Combustion Meeting*, CPIA Publication 638, vol. 1, pp. 149–159, 1995.
34. Brewster, M. Q., and T. B. Schroeder. "Experimental Study of Steady and Unsteady Combustion of RDX." *Proceedings of the 32nd JANNAF Combustion Meeting*, CPIA Publication 638, vol. 1, pp. 85–93, 1995.
35. Hanson-Parr, D., and T. Parr. "Spontaneous Raman Spectroscopy Applied to Nitramine Flames." *Proceedings of the 35th JANNAF Combustion Meeting*, in press December 1998.

INTENTIONALLY LEFT BLANK.

<u>NO. OF COPIES</u>	<u>ORGANIZATION</u>	<u>NO. OF COPIES</u>	<u>ORGANIZATION</u>
2	DEFENSE TECHNICAL INFORMATION CENTER DTIC DDA 8725 JOHN J KINGMAN RD STE 0944 FT BELVOIR VA 22060-6218	1	DIRECTOR US ARMY RESEARCH LAB AMSRL DD 2800 POWDER MILL RD ADELPHI MD 20783-1197
1	HQDA DAMO FDT 400 ARMY PENTAGON WASHINGTON DC 20310-0460	1	DIRECTOR US ARMY RESEARCH LAB AMSRL CI AI R (RECORDS MGMT) 2800 POWDER MILL RD ADELPHI MD 20783-1145
1	OSD OUSD(A&T)/ODDDR&E(R) R J TREW THE PENTAGON WASHINGTON DC 20301-7100	3	DIRECTOR US ARMY RESEARCH LAB AMSRL CI LL 2800 POWDER MILL RD ADELPHI MD 20783-1145
1	DPTY CG FOR RDA US ARMY MATERIEL CMD AMCRDA 5001 EISENHOWER AVE ALEXANDRIA VA 22333-0001	1	DIRECTOR US ARMY RESEARCH LAB AMSRL CI AP 2800 POWDER MILL RD ADELPHI MD 20783-1197
1	INST FOR ADVNCD TCHNLGY THE UNIV OF TEXAS AT AUSTIN PO BOX 202797 AUSTIN TX 78720-2797		<u>ABERDEEN PROVING GROUND</u>
1	DARPA B KASPAR 3701 N FAIRFAX DR ARLINGTON VA 22203-1714	4	DIR USARL AMSRL CI LP (BLDG 305)
1	US MILITARY ACADEMY MATH SCI CTR OF EXCELLENCE MADN MATH MAJ HUBER THAYER HALL WEST POINT NY 10996-1786		
1	DIRECTOR US ARMY RESEARCH LAB AMSRL D D R SMITH 2800 POWDER MILL RD ADELPHI MD 20783-1197		

NO. OF  
COPIES

ORGANIZATION

ABERDEEN PROVING GROUND

36 DIR USARL  
AMSRL WM BD  
W R ANDERSON  
R A BEYER  
A BIRK  
A L BRANT  
S W BUNTE  
C F CHABALOWSKI  
L M CHANG  
T P COFFEE  
J COLBURN  
P J CONROY  
R A FIFER  
B E FORCH  
B E HOMAN (5 CPS)  
S L HOWARD  
P J KASTE  
A J KOTLAR  
C LEVERITT  
K L MCNESBY  
M MCQUAID  
M S MILLER  
T C MINOR  
A W MIZIOLEK  
J B MORRIS  
J A NEWBERRY  
M J NUSCA  
R A PESCE-RODRIGUEZ  
G P REEVES  
B M RICE  
R C SAUSA  
J A VANDERHOFF  
A W WILLIAMS

<u>NO. OF COPIES</u>	<u>ORGANIZATION</u>	<u>NO. OF COPIES</u>	<u>ORGANIZATION</u>
1	DIRECTOR US ARMY RESEARCH OFFICE AMXRO RT IP LIB SERVICES RESEARCH TRIANGLE PARK NC 27709	1	UNIV OF CALIFORNIA LOS ALAMOS SCIENTIFIC LAB PO BOX 1663 MS B216 LOS ALAMOS NM 91125
1	COMMANDER NAVAL WEAPONS CENTER T PARR CODE 3895 T BOGGS CODE 388 CHINA LAKE CA 93555-6001	1	CORNELL UNIV DEPT OF CHEMISTRY T COOL BAKER LABORATORY ITHICA NY 14853
1	BRIGHAM YOUNG UNIV DEPT OF CHEMICAL ENGR M W BECKSTEAD PROVO UT 84058	1	PRINCETON UNIV FORRESTAL CAMPUS LIB PO BOX 710 PRINCETON NJ 08540
1	UNIV OF DELAWARE CHEMISTRY DEPT T BRILL NEWARK DE 19711	1	RENSSELAER POLYTECHNIC INST DEPT OF CHEMICAL ENGR A FONTIJN TROY NY 12181
4	PENN STATE UNIV DEPT OF MECH ENGR K KUO V YANG A ULAS 140 RESEARCH BLVD EAST UNIVERSITY PARK PA 16802		
4	COMMANDER US ARMY ARDEC SMCAR AEE D S DOWNS L HARRIS T MANNING S MOY PICATINNY ARSENAL NJ 07806-5000		
1	COMMANDER NAVAL RESEARCH LAB M C LIN WASHINGTON DC 20375		
1	COMMANDANT USAFAS ATSF TSM CN FORT SILL OK 73503-5600		

INTENTIONALLY LEFT BLANK.

<b>REPORT DOCUMENTATION PAGE</b>			<i>Form Approved</i> <i>OMB No. 0704-0188</i>		
Public reporting burden for this collection of information is estimated to average 1 hour per response, including the time for reviewing instructions, searching existing data sources, gathering and maintaining the data needed, and completing and reviewing the collection of information. Send comments regarding this burden estimate or any other aspect of this collection of information, including suggestions for reducing this burden, to Washington Headquarters Services, Directorate for Information Operations and Reports, 1215 Jefferson Davis Highway, Suite 1204, Arlington, VA 22202-4302, and to the Office of Management and Budget, Paperwork Reduction Project(0704-0188), Washington, DC 20503.					
1. AGENCY USE ONLY (Leave blank)		2. REPORT DATE April 2001	3. REPORT TYPE AND DATES COVERED Final, January 1998 - December 1999		
4. TITLE AND SUBTITLE On the Flame Structure of RDX			5. FUNDING NUMBERS 611102AH43		
6. AUTHOR(S) Barrie E. Homan, Martin S. Miller, and John A. Vanderhoff					
7. PERFORMING ORGANIZATION NAME(S) AND ADDRESS(ES) U. S. Army Research Laboratory ATTN: AMSRL-WM-BD Aberdeen Proving Ground, MD 21005-5066			8. PERFORMING ORGANIZATION REPORT NUMBER ARL-TR-2444		
9. SPONSORING/MONITORING AGENCY NAMES(S) AND ADDRESS(ES)			10.SPONSORING/MONITORING AGENCY REPORT NUMBER		
11. SUPPLEMENTARY NOTES					
12a. DISTRIBUTION/AVAILABILITY STATEMENT Approved for public release; distribution is unlimited.			12b. DISTRIBUTION CODE		
13. ABSTRACT (Maximum 200 words) <p>In an attempt to refine the database for the evaluation of detailed-chemistry combustion models, absorption spectroscopy has been applied to low pressure, self-deflagrating RDX flames. Semi-empirically determined production rates of reactants from the solid propellant surface, together with a detailed gas-phase elementary reaction set, were used to develop a model that minimizes the effect of uncertainties in the description of solid phase processes. The spatial profiles of two low concentration, highly reactive, short-lived diatomic species, CN and NH, were obtained at pressures varying from 1 to 2 atm in air. Two major species, NO and OH, were also profiled using this technique. The CN and NH profiles agree well with previous measurements and the current model. NO and OH profiles are also in good agreement with the models. During the course of these spectroscopic measurements, burning rates for RDX over a pressure range of 1-2 atm have also been determined. These values range from 0.23 mm/s at atmospheric pressure to 0.50 mm/s for 2 atm and are noticeably lower than some of the other published measurements. Calculations stemming from the proposed model predict a burning rate of 0.29 mm/s and 0.54 mm/s for the same pressure levels.</p>					
14. SUBJECT TERMS RDX, combustion, diagnostics, burning rate, modeling, absorption, NO, CN, NH, OH			15. NUMBER OF PAGES 39		
			16. PRICE CODE		
17. SECURITY CLASSIFICATION OF REPORT UNCLASSIFIED	18. SECURITY CLASSIFICATION OF THIS PAGE UNCLASSIFIED	19. SECURITY CLASSIFICATION OF ABSTRACT UNCLASSIFIED	20. LIMITATION OF ABSTRACT UL		

INTENTIONALLY LEFT BLANK.

**USER EVALUATION SHEET/CHANGE OF ADDRESS**

This Laboratory undertakes a continuing effort to improve the quality of the reports it publishes. Your comments/answers to the items/questions below will aid us in our efforts.

1. ARL Report Number/Author ARL-TR-2444 (Homan) Date of Report April 2001

2. Date Report Received \_\_\_\_\_

3. Does this report satisfy a need? (Comment on purpose, related project, or other area of interest for which the report will be used.) \_\_\_\_\_

4. Specifically, how is the report being used? (Information source, design data, procedure, source of ideas, etc.) \_\_\_\_\_

5. Has the information in this report led to any quantitative savings as far as man-hours or dollars saved, operating costs avoided, or efficiencies achieved, etc? If so, please elaborate. \_\_\_\_\_

6. General Comments. What do you think should be changed to improve future reports? (Indicate changes to organization, technical content, format, etc.) \_\_\_\_\_

CURRENT ADDRESS

Organization \_\_\_\_\_

Name \_\_\_\_\_ E-mail Name \_\_\_\_\_

Street or P.O. Box No. \_\_\_\_\_

City, State, Zip Code \_\_\_\_\_

7. If indicating a Change of Address or Address Correction, please provide the Current or Correct address above and the Old or Incorrect address below.

OLD ADDRESS

Organization \_\_\_\_\_

Name \_\_\_\_\_

Street or P.O. Box No. \_\_\_\_\_

City, State, Zip Code \_\_\_\_\_

(Remove this sheet, fold as indicated, tape closed, and mail.)  
**(DO NOT STAPLE)**

---

DEPARTMENT OF THE ARMY

OFFICIAL BUSINESS

**BUSINESS REPLY MAIL**  
FIRST CLASS PERMIT NO 0001,APG,MD

POSTAGE WILL BE PAID BY ADDRESSEE

DIRECTOR  
US ARMY RESEARCH LABORATORY  
ATTN AMSRL WM BD  
ABERDEEN PROVING GROUND MD 21005-5066



NO POSTAGE  
NECESSARY  
IF MAILED  
IN THE  
UNITED STATES

